Magnetotelluric monitoring of a fluid injection: Example from an enhanced geothermal system

J. R. Peacock,[1] S. Thiel,[1] P. Reid,[2] and G. Heinson[3]

Received 12 July 2012; accepted 13 August 2012; published 21 September 2012.

[1] Enhanced geothermal systems (EGS) are on the verge of becoming commercially viable for power production, where advancements in subsurface characterization are imperative to develop EGS into a competitive industry. Theory of an EGS is simple, pump fluids into thermally enhanced lithology and extract the hot fluids to produce energy. One significant complication in EGS development is estimating where injected fluids flow in the subsurface. Micro-seismic surveys can provide information about where fractures opened, but not fracture connectivity nor fluid inclusion. Electromagnetic methods are sensitive to conductivity contrasts and can be used as a supplementary tool to delineate reservoir boundaries. In July, 2011, an injection test for a 3.6 km deep EGS at Paralana, South Australia was continuously monitored by both micro-seismic and magnetotellurics (MT). Presented are the first results from continuous MT measurements suggesting transient variations in subsurface conductivity structure generated from the introduction of fluids at depth can be measured. Furthermore, phase tensor representation of the time dependent MT response suggests fluids migrated in a NE direction from the injection well. Results from this experiment supports the extension of MT to a monitoring tool for not only EGS but other hydraulic stimulations. **Citation:** Peacock, J. R., S. Thiel, P. Reid, and G. Heinson (2012), Magnetotelluric monitoring of a fluid injection: Example from an enhanced geothermal system, *Geophys. Res. Lett.*, *39*, L18403, doi:10.1029/2012GL053080.

1. Introduction

[2] Novel technologies need to be developed to facilitate the switch in energy production from fossil fuels to renewable energy. One promising technology on the verge of becoming economically viable is enhanced geothermal systems (EGS) [*Tester et al.*, 2006]. Initially tested at Fenton Hill, New Mexico in the 1970's, EGS is attractively simple. First, pump fluids into thermally enhanced lithology to generate a reservoir, where heat is absorbed by the fluids. Then, extract the hot fluids to produce energy. Unfortunately, realizing this simple idea proves to be complex due to numerous unknowns in the subsurface [*Brown*, 1995]. One major unknown is tracking and characterizing location of fluids introduced into the lithology through hydraulic stimulation. The main technique for monitoring EGS reservoir development is micro-seismic [*Wohlenberg and Keppler*, 1987; *House*, 1987], where tomography locates earthquakes associated with fractures caused by hydraulic pressure and shear wave splitting can estimate size and orientation of the fractures [*Rial et al.*, 2005]. However, the micro-seismic technique is not directly sensitive to fluid inclusion nor connectivity of the fractures.

[3] Electromagnetic methods are sensitive to electrical conductivity contrasts at depth, including the presence of hot, saline, and electrically conductive fluids well connected in a resistive host rock. With typical depths of an EGS deeper than 3 km, magnetotellurics (MT) becomes an advantageous choice because of its versatile depth of investigation. MT is a passive technique that measures the Earth's electrical response to natural time varying magnetic fields, formally linked by the linear MT transfer function **Z**, where depth of investigation and resolution depends directly on the period of the inducing magnetic field [*Kaufman and Keller*, 1981]. Therefore, MT cannot directly measure individual fractures, only bulk volumetric conductivity contrasts assumed to be fluid filled fracture networks in an EGS sense. In geothermal applications, MT is typically applied as an exploration tool to characterize and locate potential geothermal targets [e.x., *Heise et al.*, 2008; *Newman et al.*, 2008; *Spichak and Manzella*, 2009; *Arango et al.*, 2009]. Utility of MT as a monitoring tool has predominantly been applied to searching for the elusive electromagnetic precursors to earthquakes [*Kappler et al.*, 2010]. However, a recent study by *Aizawa et al.* [2011] demonstrates MT can monitor temporal variations in subsurface electrical conductivity associated with geothermal fluid movement. In one of the first MT surveys designed to monitor a fluid stimulation for an EGS, *Bedrosian et al.* [2004] found MT data did not measure a coherent change in subsurface conductivity caused by injected fluids because cultural noise influenced much of the data and the conductive overburden absorbed most of the electromagnetic energy. Additionally, *Bedrosian et al.* [2004] conducted a forward modeling exercise and found a conductive body on the order of 1 km^2 at 4 km depth would be detectable by MT. Notwithstanding, forward modeling and feasibility studies can only forecast plausible outcomes not exactly predict experimental results. Presented in this paper are pioneering results from continuous MT measurements that show coherent changes above measurement error generated from a fluid injection experiment designed to create the first stage of an EGS at Paralana, South Australia.

2. Measurement

[4] In July, 2011, for their EGS project at Paralana, South Australia, Petratherm Ltd. injected 3.1 million liters of saline

[1]South Australian Centre for Geothermal Energy Research, University of Adelaide, Adelaide, South Australia, Australia.
[2]Petratherm Ltd., Adelaide, South Australia, Australia.
[3]TRaX, Department of Geology and Geophysics, University of Adelaide, Adelaide, South Australia, Australia.

Corresponding author: J. R. Peacock, Department of Geology and Geoscience, University of Adelaide, Mawson Building, Adelaide, SA 5005, Australia. (jared.peacock@adelaide.edu.au)

0094-8276/12/2012GL053080

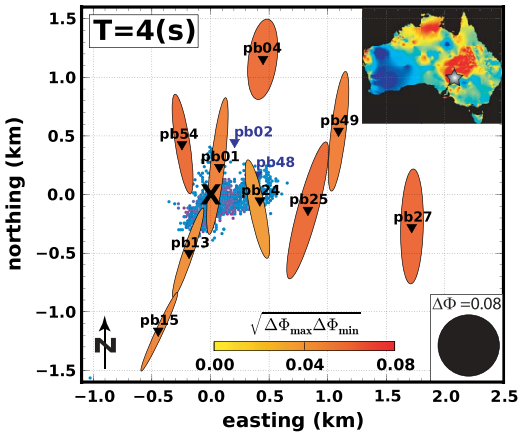

Figure 1. Map of Paralana, South Australia displaying MT station locations (triangles) centered on Paralana 2 injection well (X), and micro-seismic events measured during the injection experiment from *Hasting et al.* [2011] (circles colored by day–192 as red to 196 blue). Top right is a temperature map of Australia from Geoscience Australia at 5 km depth where reds represent 285 C and the gray star locates Paralana. Stations that malfunctioned are colored blue and are not used in this analysis. The ellipses represent phase tensor residuals (1) of pre-injection and day 196 for a period of 4 s. The face color is estimated as $\sqrt{\Delta\Phi_{max}\,\Delta\Phi_{min}}$ [*Heise et al.*, 2008]. Interestingly, ellipse orientation generally aligns with the seismic cloud, suggesting that fluctuations in the MT response correlate with geoelectric alteration provoked by connected fluid filled pathways developed during the injection experiment.

water (resistivity of 0.3 Ω·m) into a Mesoproterozoic metasedimentary package at 3680 m depth through an 6 m perforated zone of the cased Paralana 2 borehole. The injection took 4 days to complete, starting on day 193 at 0400 universal time (UT) with low flow rates (2 barrels per minute) followed by a sequence of shutting in and increasing flow rates step wise to a maximum of 16 barrels per minute. Pumping concluded on day 196 at 0400 UT when the well was shut in. A micro-seismic array measured over 11,000 events suggesting the fractures opened in a NE preferred direction, with the majority located in the NE quadrant from the Paralana 2 borehole [*Hasting et al.*, 2011] (colored circles in Figure 1). Two days before the injection, 11 broadband 4-component AuScope MT instruments were placed around the Paralana 2 borehole; the furthest station being about 2 km away (Figure 1). Survey design was based on a previous injection test that showed fracturing tendency to be NE of the borehole. MT instruments recorded for an entirety of 8 days, including 2 days pre-injection, 4 days during injection and 2 days post-injection. A solar powered AuScope instrument was set up 60 km south of Paralana as a remote reference. Instruments sampled at 500 Hz and were synchronized by GPS. Dipoles were approximately 50 m in length, employing Cu-$CuSO_4$ non-polarizing porous pots as electrodes laid out in an L-shape aligned with geomagnetic north, which is fortuitously also regional geoelectric strike. Data were retrieved from the instruments every day to ensure data quality, while instrument setup was checked for functional completeness and batteries where changed every third day.

3. Data Processing and Analysis

[5] Time series were checked for quality and coherent noise using robust time-frequency analysis formalized by *Djurovic et al.* [2003]. Magnetic source field effects were estimated using a principal component analysis similar to *Egbert* [1997], finding only two dominant principal components except for a window of 1400–2400 on UT day 194. MT transfer functions were estimated for 1, 4, 6, 12, and 24 hour blocks utilizing a robust bounded influence remote referencing method developed by *Chave and Thomson* [2004]. As source field power was low in the MT dead band (1–10 s) during local night time, a magnetic coherency threshold between the station and remote reference station was applied to remove influence of non-coherent and weakly coherent signal on **Z** that might produce false anomalies [*Mareschal*, 1986]. Coherency between measured electric fields and predicted electric fields from measured magnetic fields was maximum across all periods for **Z** calculated using 24 hour blocks. Estimated mean error for **Z** of 24 hour blocks is approximately 1.4 percent, while average repeatability of MT parameters for the period range .01–1 s is within 0.4 percent between 24 hour blocks. Therefore, the following data analysis is focused on **Z** calculated from 24 hour time windows.

[6] One benefit of conducting electromagnetic surveys in the Australian outback is the lack of electromagnetic noise sources, nevertheless there are other logistical aspects of data collection. Out of the 11 instruments deployed, 6 functioned consistently throughout the survey. The other 5 instruments were sporadically disrupted by mice chewing electrode cables or electrodes being dug or pulled out by other animals. These time windows of poor data quality are not used to estimate **Z**. Stations pb02 and pb48 are not used in this analysis because they malfunctioned too often to estimate reliable transfer functions. Other noise sources include pumps used for the injection (operating at periods of ∼1 s and ∼6 s) and site specific noise. Fortunately, influence from these noise sources is minimal in these data. Also, it is important to note that the residuals, calculated as the MT response pre-injection minus each 24 hour time window, are calculated for each station. Therefore, any time invariant systematic noise, such as instrument noise, will be subtracted out. Near surface distortion is estimated and removed following *Bibby et al.* [2005]. Note the phase tensor is invariant to near surface distortions, making it an advantageous parameter to represent the MT response [*Caldwell et al.*, 2004].

[7] Variations in MT parameters are estimated by computing residuals of pre-injection MT parameters minus subsequent 24 hour blocks, specifically for apparent resistivity, impedance phase and the phase tensor parameters (see auxiliary material).[1] Phase tensor residuals provide information about geoelectric strike transformation during the injection and gradients in resistivity structure, suggesting reservoir boundaries. Here the phase tensor residuals are

[1]Auxiliary materials are available in the HTML. doi:10.1029/2012GL053080.

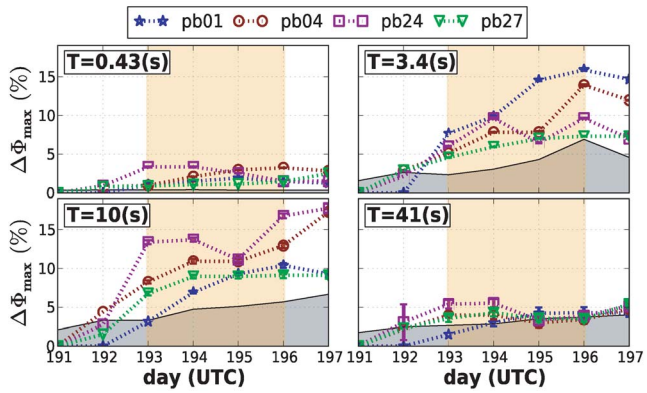

Figure 2. Plots of percent change in Φ_{max} (an invariant of (1), see *Caldwell et al.* [2004]) as a function of time for selected stations and periods (T). The shaded gray region is the estimated error floor as a function of time and period, giving a baseline to which variations can be confidently estimated and interpreted. The shaded orange region designates the pumping period when fluids were injected into the subsurface. Notice that periods between 1–10 s experience a general increasing change above the error floor, while periods outside this band do not.

calculated as a percent change (1), where Φ_o is the phase tensor pre-injection, Φ_j is the phase tensor of a 24 hour block, $\mathbf{I}$ is the identity matrix of rank two and $\mathbf{\Phi}^{-1}$ is the inverse. The face color can be represented as the geometric mean $\sqrt{\Delta\Phi_{max}\ \Delta\Phi_{min}}$ [*Heise et al.*, 2008]. For more on phase tensor behavior in anisotropic media see *Heise et al.* [2006] and *Caldwell et al.* [2004]. Finally, to ensure bulk changes are estimated robustly, a median filter is applied to the each MT parameter, calculating the single station median for three periods at three different times.

$$\Delta\Phi oj = \mathbf{I} - \left(\mathbf{\Phi}_o^{-1}\mathbf{\Phi}_j\right). \quad (1)$$

4. Discussion

[8] First and foremost, confidence in variations of the MT response must be instilled before any in depth interpretation can begin. The first thing to look for is a clear separation between the MT response pre-injection and MT responses estimated at later times. This provides an indication of variational magnitude and suggests a confidence level that observable temporal changes beyond measurement error exist. The second pattern to look for is causality, where variations in impedance phase should predict apparent resistivity changes according to the dispersion relation [*Berdichevsky and Dmitriev*, 2008]. Specifically for a conductive change at 3.6 km at Paralana, the phase should increase at ~1–10 s and the apparent resistivity should decrease beyond ~8 s. The general trend for most stations is for the apparent resistivity is reduced below periods of 8 s and the phase increases around 1–10 s for MT responses estimated during the injection (see auxiliary material). Moreover, most of these changes are near or just above the measurement error where variational magnitude is larger in the Z_{xy} than the orthogonal polarization, suggesting that change in geoelectric structure has a preferred direction towards the North. However, not all stations have consistent measurable changes above the noise level, therefore those that did will be discussed, namely pb01, pb04, pb24 and pb27. The others had intermittent periods where mice chewed cables or electrodes got pulled out by curious marsupials.

[9] Another method to provide confidence in observable changes is to estimate an error floor by propagating an error estimate to each MT parameter, assuming that the error is identically 1D. An error estimate can be calculated as the ratio of the sum of the error in estimation of $\mathbf{Z}$ and repeatability divided by $\mathbf{Z}$ as a function of period and time for each station; this gives a percent change confidence floor. Applying a median filter and taking the maximum percent change estimate as a function of time and frequency of the aforementioned stations provides a robust baseline to which MT parameters can be compared to. Specifically, if the residual in the MT parameter is above this baseline then it can confidently be analyzed as a measurable signal (Figure 2). Estimating parameters of the phase tensor [*Caldwell et al.*, 2004] provides dimensionality information and a representation of the MT response that is insensitive to distortions. Phase tensor representation of the time dependent $\mathbf{Z}$ suggests a general trend of increase in $\Delta\Phi_{max}$ as a function of time between 1–10 s, conversely $\Delta\Phi_{min}$ does not change above the error floor, again suggesting a directional dependence. Interestingly, for periods in the dead band (1–10 s), the error floor displays an increasing linear trend from the start date to the end date. However, magnetic source field power did not decrease from start to finish enough to cause an increase in error of estimating $\mathbf{Z}$. Moreover, electrical noise from mechanical pumps (1 s and 6 s) remained nearly constant for the pumping period. Similarly, cathodic protection from the EPIC pipeline (2 km west of injection well see Figure 1) was time-invariant. A plausible explanation is that the subsurface sampled at periods between 1–10 s (skin depth of ~3–8 km) became more conductive over the duration of pumping due to the injection of saline fluids. This would cause a decrease in electric field strength at those periods and cause a decrease in coherency between the measured electric and magnetic field, propagating into an uncertainty increase in the estimation of $\mathbf{Z}$.

[10] Estimating depth to the conductive anomaly can ensure the change is occurring at the correct depth. An 1D Occam inversion [*Key*, 2009] of the mode where the electric field is aligned with maximum change estimates a depth of 2.8–3.3 km. Though it was found that inverting synthetic data estimated with a conductive anomaly at 3.6 km in a similar way found a depth of 3.3 km as well. A 2D Occam inversion [*Constable et al.*, 1987] can be employed to estimate depth as a function of time for each station. Here the lateral dimension is now time instead of space and stations are spaced 20 km to remove any influence of neighboring stations at the target depth. Again, only the mode where the electric field is aligned with maximum change is modeled here because of its sensitivity to subsurface electrical variations. The estimated depth is 2.8 km, which is off by about 800 m from the known depth (see auxiliary material), but nevertheless is close to the expected depth range and similar to result found from a similar exercise using synthetic data. Occam's method finds the smoothest model possible and can smooth the resistivity structure increasing the uncertainty in the depth. Similarly, because MT is an integral

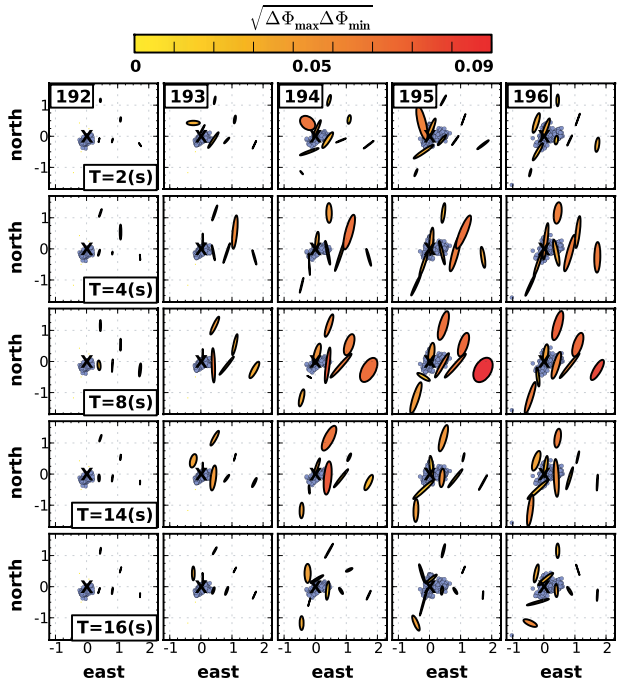

Figure 3. Maps of phase tensor residual ellipses calculated as (1) and colored as the geometric mean of (1). Each column represents one day and each row represents one period. Paralana 2 borehole is marked as an X. The seismic cloud for each day is represented as by blue circles [*Hasting et al.*, 2011]. Generally, ellipse orientation aligns with the direction of the seismic cloud, while size increases and color becomes warmer from day 193 to 196.

method, if the conductance above the body is not properly estimated the depth will also not be accurately estimated. Accuracy can be improved with other electric and electromagnetic measurements.

[11] Finally, dimensional variations in the MT response can be estimated from the residual phase tensor (1). Interestingly, phase tensor residuals are larger than forward modeling predicts (see auxiliary material) by an order of magnitude, suggesting a greater contrast between host rock and the conductive body, also supporting experimentation over feasibility studies. Three general observations can be made from phase tensor residuals represented as an ellipse. First, average ellipse orientation aligns in a NE direction from periods between 1–10 s (Figures 1 and 3). This is also the regional strike direction and orthogonal to principle stress direction suggesting a correlation between electric strike and principle stress directions. Second, larger changes are observed to the NE of the borehole. Third, for periods between 1–10 s, size of phase tensor ellipses increases and face color becomes more red with each day, imaging changing geoelectric structure due to a growing conductive body at depth. However, phase tensor orientation exhibits behavior not of a simple homogeneous conductive block, but a complicated system of heterogeneous anisotropic pathways. Further work and more experimentation needs to be done to fully understand the MT response in time-variant fractured media. These three observations correlate well with micro-seismic data showing the majority of micro earthquakes occurred NE of the borehole and elongated generally in the NE direction. It is important to note that micro-seismic data can locate fractures opening, while MT estimates volumetric changes in the geoelectric structure associated with fluid filled fracture networks. Therefore, these two geophysical techniques should be used in tandem as complementary pairs.

5. Conclusion

[12] In this experiment, MT has been successfully applied to monitoring a fluid injection for the first stage of an EGS, where changes in the MT response are assumed to originate from the injection of electrically conductive fluids connected by induced fracture networks at 3.6 km depth. Though the variations in MT parameters are on the order of a few percent, they are coherent in space and time, while being above measurement error. Furthermore, temporal and spatial variations correlate with the pumping schedule and results from a concurrent micro-seismic survey. Plotting apparent resistivity and impedance phase of pre-injection and subsequent 24 hour blocks provides visual conformation that observable changes exist above measurement error, while inverting the MT response as a function of time using a 2D algorithm is useful for estimating depth to the evolving conductive body, though absolute depth can have large errors stemming from inaccurate conductance estimation. Estimating an error floor for each MT parameter can be used as another tool to instill confidence in observable changes. Finally, mapping the phase tensor residuals prove most informative for observing temporal and spatial changes generated by a growing conductive body at depth, indicating that reservoir evolution is a complex growth to the NE of the borehole, expanding in a NE preferred orientation. Three methods to improve monitoring MT surveys are to utilize more than one remote reference to better understand regional variations in the magnetic source field [*Kappler et al.*, 2010], measure vertical magnetic fields and increase the number of stations to cover a larger area for improved lateral resolution. Positive results from this experiment demonstrate the potential of expanding MT monitoring to other fluid injections, such as non-conventional natural gas where controlled source techniques can be applied [*Orange et al.*, 2009; *Streich et al.*, 2010; *Wirianto et al.*, 2010].

[13] **Acknowledgments.** The authors would like to thank Petratherm and joint venture partners Beach Petroleum for support of this project. Mathieu Messieller, Louise McAllister, Goran Boren, Jonathan Ross, Hamish Adam, Tristan Wurst, Kiat Low, Aixa Rivera-Rios, Alison Langsford, and Kathrine Stoate for field assistance. Institute for Mineral and Energy Research, South Australian Center of Geothermal Energy Research and South Australia Department for Manufacturing, Innovation, Trade, Resources and Energy for financial support. Grant Caldwell for useful discussions on phase tensors and Mike Hatch for improving readability.

[14] The Editor thanks an anonymous reviewer for assisting in the evaluation of this paper.

References

Aizawa, K., W. Kanda, Y. Ogawa, M. Iguchi, A. Yokoo, H. Yakiwara, and T. Sugano (2011), Temporal changes in electrical resistivity at Sakurajima Volcano from continuous magnetotelluric observations, *J. Volcanol. Geotherm. Res.*, *199*, 165–175, doi:10.1016/j.jvolgeores.2010.11.003.

Arango, C., A. Marcuello, J. Ledo, and P. Queralt (2009), 3D magnetotelluric characterization of the geothermal anomaly in the Llucmajor aquifer system (Majorca, Spain), *Geothermics*, *68*, 479–488, doi:10.1016/j.jappgeo.2008.05.006.

Bedrosian, P. A., U. Weckmann, O. Ritter, C. U. Hammer, J. Hübert, and A. Jung (2004), Electromagnetic monitoring of the Groß Schönebeck

stimulation experiment, in *Jahrestagung der Deutschen Geophysikalischen Gessellschaft*, p. 64, GFZ, Berlin.

Berdichevsky, M. N., and V. I. Dmitriev (2008), *Models and Methods of Magnetotellurics*, Springer, Berlin.

Bibby, H. M., T. G. Caldwell, and C. Brown (2005), Determinable and non-determinable parameters of galvanic distortion in magnetotellurics, *Geophys. J. Int.*, *163*, 915–930, doi:10.1111/j.1365-246X.2005.02779.x.

Brown, D. (1995), The US hot dry rock program—20 years of experience in reservoir testing, in *Proceedings of the World Geothermal Congress, 1995: Florence, Italy*, pp. 2607–2611, Int. Geotherm. Assoc., Auckland, N. Z.

Caldwell, T. G., H. M. Bibby, and C. Brown (2004), The magnetotelluric phase tensor, *Geophys. J. Int.*, *158*, 457–457, doi:10.1111/j.1365-246X.2004.02203.x.

Chave, A. D., and D. J. Thomson (2004), Bounded influence magnetotelluric response function estimation, *Geophys. J. Int.*, *157*, 988–1006, doi:10.1111/j.1365-246X.2004.02203.x.

Constable, S. C., R. L. Parker, and C. G. Constable (1987), Occam's inversion: a practical algorithm for generating smooth models from electromagnetic sounding data, *Geophysics*, *52*, 289–300.

Djurovic, I., L. Stankovic, and J. F. Bohme (2003), Robust L-estimation based forms of signal transforms and time-frequency representations, *IEEE Trans. Signal Process.*, *51*, 1753–1761, doi:10.1109/TSP.2003.812739.

Egbert, G. D. (1997), Robust multiple-station magnetotelluric data processing, *Geophys. J. Int.*, *130*, 475–496, doi:10.1111/j.1365-246X.1997.tb05663.x.

Hasting, M. A., J. Albaric, V. Oye, P. Reid, M. Messeiller, and E. Llanos (2011), Micro-seismic monitoring during stimulation at Paralana-2 South Australia, Abstract H21E-1159 presented at 2011 Fall Meeting, AGU, San Francisco, Calif., 5–9 Dec.

Heise, W., T. Caldwell, H. Bibby, and C. Brown (2006), Anisotropy and phase splits in magnetotellurics, *Phys. Earth Planet. Inter.*, *158*, 107–121, doi:10.1016/j.pepi.2006.03.021.

Heise, W., T. G. Caldwell, H. M. Bibby, and S. C. Bannister (2008), Three-dimensional modelling of magnetotelluric data from the Rotokawa geothermal field, Taupo Volcanic Zone, New Zealand, *Geophys. J. Int.*, *173*, 740–750, doi:10.1111/j.1365-246X.2008.03737.x.

House, L. S. (1987), Locating microearthquakes induced by hydraulic fracturing in crystalline rock, *Geophys. Res. Lett.*, *14*, 919–921, doi:10.1029/GL014i009p00919.

Kappler, K. N., H. F. Morrison, and G. D. Egbert (2010), Long-term monitoring of ULF electromagnetic fields at Parkfield, California, *J. Geophys. Res.*, *115*, B04406, doi:10.1029/2009JB006421.

Kaufman, A. A., and G. V. Keller (1981), *The Magnetotelluric Sounding Method*, Elsevier, Amsterdam.

Key, K. (2009), 1D inversion of multicomponent, multifrequency marine CSEM data: Methodology and synthetic studies for resolving thin resistive latyers, *Geophysics*, *74*, F9–F20.

Mareschal, M. (1986), Modelling of natural sources of magnetospheric origin in the interpretation of regional induction studies: A review, *Surv. Geophys.*, *8*, 261–300, doi:10.1007/BF01904062.

Newman, G. A., R. Gasperikova, G. M. Hoversten, and P. E. Wannamaker (2008), Three-dimensional magnetotelluric characterization of the Coso geothermal field, *Geothermics*, *37*, 369–399, doi:10.1016/j.geothermics.2008.02.006.

Orange, A., K. Key, and S. Constable (2009), The feasibility of reservoir monitoring using time-lapse marine CSEM, *Geophysics*, *74*, F21–F29, doi:10.1190/1.3059600.

Rial, J. A., M. Elkibbi, and M. Yang (2005), Shear-wave splitting as a tool for the characterization of geothermal fractured reservoirs: Lessons learned, *Geothermics*, *34*, 365–385, doi:10.1016/j.geothermics.2005.03.001.

Spichak, V. V., and A. Manzella (2009), Electromagnetic sounding of geothermal zones, *J. Appl. Geophys.*, *68*, 459–478, doi:10.1016/j.jappgeo.2008.05.007.

Streich, R., M. Becken, and O. Ritter (2010), Imaging CO_2 storage sites, geothermal reservoirs, and gas shales using controlled-source magnetotellurics: Modeling studies, *Chem. Erde*, *70*, 63–75, doi:10.1016/j.chemer.2010.05.004.

Tester, J. W., et al. (2006), *The Future of Geothermal Energy*, MIT Press, Cambridge, Mass.

Wirianto, M., W. A. Mulder, and E. C. Slob (2010), A feasibility study of land CSEM reservoir monitoring in a complex 3-D model, *Geophys J Int*, *181*, 741–755, doi:10.1111/j.1365-246X.2010.04544.x.

Wohlenberg, J., and H. Keppler (1987), Monitoring and interpretation of seismic observations in hot dry rock geothermal energy systems, *Geothermics*, *16*, 441–445, doi:10.1016/0375-6505(87)90025-3.